# AERODYNAMIC CALCULATION OF COMPLEX THREE-DIMENSIONAL CONFIGURATIONS

F. Roggero and R. Larguier
Office National d'Etudes et de Recherches Aérospatiales
Châtillon, France

## Abstract

The three-dimensional ECOPAN code was developed at ONERA to meet a wide variety of demands, including those of the Ariane and Airbus European programs. For these types of configurations, the panel method approach is still the most efficient tool as it uses only a surface grid which is relatively easy to generate. In addition recent developments of the method also make it possible to evaluate such complex configurations aerodynamically in reasonable computing time. Typical configurations are a complete launch vehicle in takeoff phase or a complete aircraft with engines operating and high lift devices extended.

In these two cases, the ECOPAN code has demonstrated is versatility, its operational status, and its aptitude to perform parametric analyses in subsonic flow with:
- Interaction of the Hermes shuttle on the lower part of the Ariane 5 launcher, correctly expressed.
- The lift increase due to the ground effect for an Airbus in takeoff, estimated to within 4 %.

## I. Introduction

The three-dimensional ECOPAN code was developed at ONERA to meet a wide variety of demands, including those of the Ariane and Airbus European programs. For these types of configurations, the panel method approach is still the most efficient tool as it uses only a surface grid which is relatively easy to generate. In addition recent developments of the method also make it possible to evaluate such complex configurations aerodynamically in reasonable computing time.

In this paper, the ECOPAN method is first briefly presented. This three-dimensional steady inviscid flow calculation code is based on research by C. Rehbach at ONERA on "inner Dirichlet" code, and has been perfected by C. Kirrmann[1] and F. Roggero.

In this method, the boundary condition used concerns the inner potential whose value is chosen so that the potential remains regular outside the bodies, thereby making the method less sensitive to the mesh irregularity than the codes using Neumann type boundary conditions.

So the inner Dirichlet condition provides a very good mass flow conservation for guided flows, minimizes leakage through the surfaces in strong interaction zones and removes the defects in the calculation of surfaces with concave areas, such as wings with supercritical profiles.

This type of method appeared around 1979 in the USA and is now widely used[2, 3]. Most new panel codes, like the VSAERO code from A.M.I[4-8], QUADPAN from Lockheed[9], S-SUB2[10], HISSS from MBB[11] ... are based on this new formulation, or at least they contain it as an option or as a particular case of a more general solution, as in the PAN'AIR code of Boeing[12,13].

A validation study is then presented by comparing ECOPAN results with those of an ONERA finite element code, for the DLR F4 civilian aircraft wing and an open engine nacelle. Some comparisons are also made with wind tunnel tests on the Hermes European shuttle.

To illustrate the code capabilities, two typical applications are presented for complex configurations:
- The future European Ariane 5 launch vehicle has been evaluated in its subsonic flight phase with and without the Hermes shuttle.
- A complete Airbus type aircraft geometry has been calculated with flaps and slats extended in takeoff configuration.

## II. ECOPAN code presentation

The ECOPAN code is used to compute subsonic inviscid flows around three-dimensional bodies such as launchers or complete aircraft.

It is an integral type method, based on the solution of the Laplace equation applied to the velocity potential:

$$\Delta \Phi = 0 \quad \text{with} \quad \vec{V} = \vec{\nabla} \Phi \tag{1}$$

The part of the flow potential that is due to the body is modeled by surface distributions of combined doublet-source panels that are elementary solutions of the Laplace equation.

### Basic integral equation for the thick body case

For a closed surface S, the application of the third Green equation (Green-Ostrogradski theorem or divergence formula:

$$\iiint \vec{\nabla}.\vec{f}\,dV = \iint \vec{n}.\vec{f}\,dS$$

applied to the vector field $\vec{f} = \phi\,\vec{\nabla}(1/r) - \vec{\nabla}\phi/r)$ gives an integral equation between the potential at a point $P$ and the source and doublet strength over $S$:

$$\Phi(P) = \frac{1}{4\pi} \iint_S \mu\,\vec{n}\vec{\nabla}_Q\left(\frac{1}{r}\right) dS_Q - \frac{1}{4\pi} \iint_S \frac{\sigma}{r}\, dS_Q + \Phi_\infty(P) \tag{2}$$

with $\mu = \phi_e - \phi_i$ doublet strength (3)

$\sigma = \vec{n}(\vec{\nabla}\phi_e - \vec{\nabla}\phi_i)$ source strength (4)

$\phi_e$ outer potential

$\phi_i$ inner potential

$r = |\vec{X}_Q - \vec{X}_P|$

The source and doublet strengths $\sigma$ and $\mu$ being unknown, the solution requires two boundary conditions.

Boundary conditions

The ECOPAN code uses an inner Dirichlet condition, which consists in imposing the potential of the virtual inside flow, in addition to the condition on the external normal velocity.

This way the sources take explicit values that depend on external normal velocities and the doublets are the solution of an integral equation prescribing the condition on the inner potential.

We usually set an inner potential corresponding to freestream boundary conditions, i.e.:

$$\phi_i = \phi_\infty \tag{5}$$

Source strengths

Equation (4) says that the source strengths are equal to the difference between outside and inside normal velocities

$$\sigma = \vec{V}_e.\vec{n} - \vec{V}_i.\vec{n} \tag{6}$$

In the case of a surface with no mass through flow the boundary conditions $\phi_i = \phi_\infty$ and $\vec{V}_e.\vec{n} = 0$ determine the source strength:

$$\sigma = -\vec{V}_\infty.\vec{n} \tag{7}$$

It is possible to impose a nontangential velocity on the body surface by means of a normal velocity condition of the form: $\vec{V}_e.\vec{n} = V_{en}$

$V_{en}$ being the local value of the given velocity, set equal to zero when the slip condition is desired and not zero in the case of a surface with a mass flow condition, for example to simulate a boundary layer by a transpiration model, or a mass flow through an engine nacelle.

Doublet strengths

The doublet strengths are obtained writing the boundary conditions (5) inside the body:

$$\underbrace{\frac{1}{4\pi}\iint_S \mu\,\vec{n}\vec{\nabla}\left(\frac{1}{r}\right)dS}_{\text{potential induced by the doublets of unknown strengths } \mu} = \underbrace{\frac{1}{4\pi}\iint_S \frac{\sigma}{r}\,dS}_{\text{known term}} \qquad \forall P \in S;$$

In a discretized form, this equation gives a linear system of the form:

$$[A]\,[\mu] = [W]$$

where $[A]$ is a square matrix, the terms of which - called influence coefficients - depend only on the body geometry, $[\mu]$ is the unknown doublet strength vector, and the second member $[W]$, which prescribes the boundary conditions, is a known vector.

This resulting linear system, in which the unknows are the doublet strengths, is solved by an L.U. bloc method with asynchronous input/output. As the rank of such systems with full matrices can exceed 10 000, complete overlapping between computation and input/output considerably diminishes the cost[14].

Velocity calculation

The inner Dirichlet condition allows a very fast calculation of the surface velocities; so it is sufficient to add to the imposed inside velocity, the normal and tangential velocity jumps, due to the source and doublet distributions.

$$\vec{V}_e = \vec{V}_i + \sigma\vec{n} + (\vec{\nabla}\mu)_S$$

and

$$\vec{V}_e = \vec{V}_\infty + \sigma\vec{n} + (\vec{\nabla}\mu)_S$$

$(\vec{\nabla}\mu)_S$ being the surface gradient of the doublet strength.

Wakes

The wing vortex sheets are discretized by wake doublet panels, equivalent to a vortex lattice extending infinitely downstream. The vortex circulation is calculated by applying an emission condition (equivalent to a Kutta-Joukowski condition) at the trailing edge of every profile. Different options are available to express this last condition, according to whether or not the trailing edge is thick and whether or not the emission condition is linearized.

Code extensions

A Prandtl-Glauert compressibility correction can be used for calculating slightly compressible flows. For complex configurations, a free-wake geometry calculation option can be used, but this is a costly iterative calculation.

Particular case of thin surfaces

When the thickness of the obstacle can be neglected, a Neumann condition is used to solve the singularity strength by a normal velocity condition on constant-strength doublet type panels. The doublet strengths are obtained solving the boundary condition on the surface:

$$\vec{v}.\vec{n} = V_{en} - \vec{n}.\vec{V}_\infty$$

in the form:

$$\underbrace{\iint_{S_b+S_e} \vec{v}_\mu.\vec{n}\,dS}_{\text{velocity induced by doublets of unknown strengths } \mu} = \underbrace{V_{en} - \vec{n}.\vec{V}_\infty - \iint_{S_b} \vec{v}_\sigma.\vec{n}\,dS}_{\text{known term}}$$

Instead of stipulating a Kutta-Joukowski type condition, this formulation is used to regulate the exit velocity in the exhaust plane of an engine nacelle directly, by adding in this plane a doublet surface that is regulated by a Neumann condition setting the value of the normal velocity at collocation points (Fig. 1).

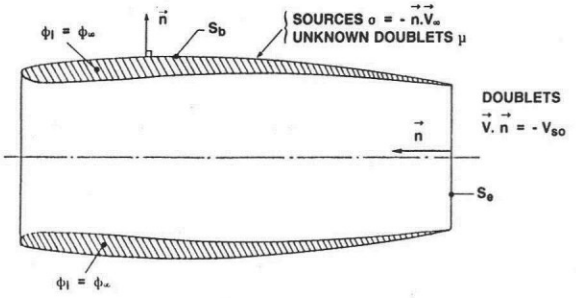


*Fig. 1. Schematic representation of an engine nacelle calculation with mass-flow control.*

Computation time

The Figure 2 shows an averaged estimation of the total computation time as a function of the number of panels, for a lifting computation with an implicit symmetry. This time is given in seconds on a CRAY XMP 18 processor. It may vary with the configuration considered and the desired options.

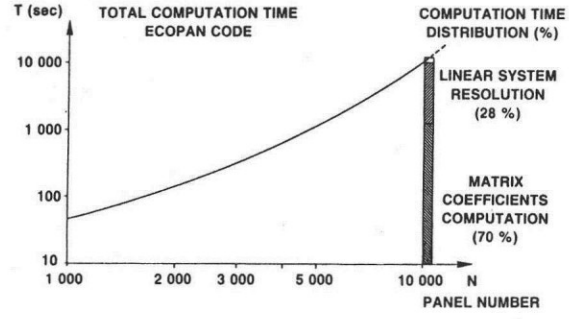


*Fig. 2. Estimation of the ECOPAN computation time on a CRAY XMP 18 processor.*

For example, the time is diminished in the case of a nonlifting computation or without specifying an implicit plane of symmetry; but it may increase if more wake lattice panels are used. An analysis of the times spent on each of the main computation phases is also shown in this figure.

## III. ECOPAN code validation

### Comparison with finite element code

#### Calculation of the DLR F4 wing

The DLR F4 research wing of transport aircraft type was calculated by ECOPAN using the grid presented in Fig. 3, and was compared with a calculation by finite element method[15], for two Mach numbers, $M = 0$ and $M = 0.3$.

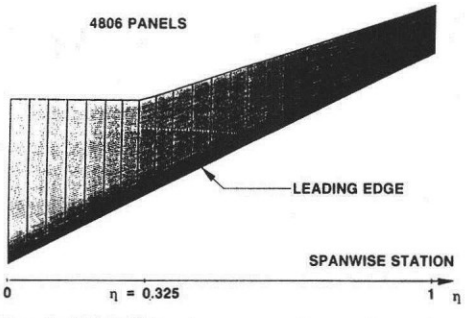


*Fig. 3. DLR F4 wing geometry and mesh.*

Figures 4 and 5 show the local pressure distribution at the wingspan section $\eta = 0.325$, and the spanwise distribution of the normal force $C_{N\eta}$ ($\eta$) for $M = 0$.

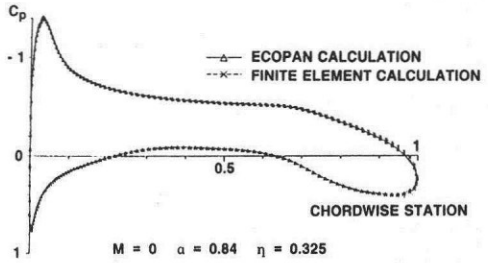


*Fig. 4. DLR F4 wing chordwise pressure distribution.*

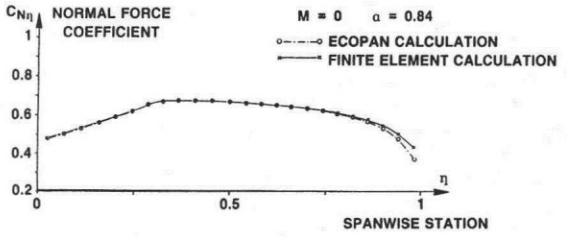


*Fig. 5. DLR F4 wing spanwise normal force distribution.*

Figure 6 presents the relative discrepancies in normal force coefficient between $M = 0$ and $M = 0.3$, as a percent. It may be noted that the compressible flow effects are quite similar for the two codes ($\Delta C_{N\eta}/C_{N\eta}$ between 3 % and 4 %).

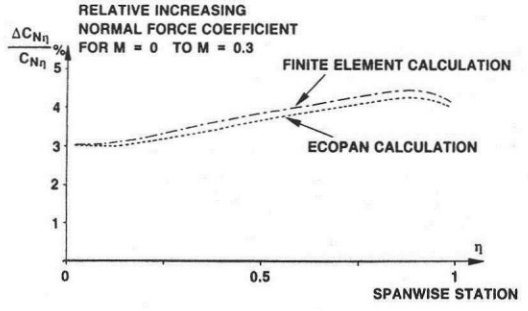


*Fig. 6. DLR F4 wing spanwise compressibility effect.*

#### Calculation of an open engine nacelle

The flow through an open engine nacelle (geometry shown in Fig. 1) was also calculated, to validate the method for guided flow[1].

The two-dimensional axisymmetric finite element method finds an exit mean velocity $V_S = 0.865$, quite similar to the value obtained by the ECOPAN method if a velocity of $V_{S0} = 0.90$ is specified at the exhaust plane. The comparisons presented in Figure 7 are thus made for constant exit mass flow.

The pressures obtained by the two methods compare well; only the leading edge peaks (inside and outside) present any noticeable discrepancy. This may be a result of the differences in grid precision (exactly axisymmetric mesh of 128 grids per profile for the finite element method, but 12 sections of 66 cosine type panels for the ECOPAN method).

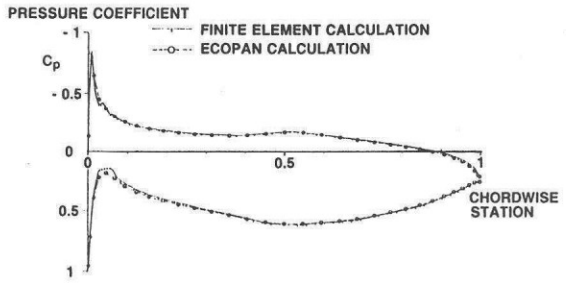


*Fig. 7. Pressure distribution on an axisymmetric open engine nacelle.*

Comparison with experimental results: computation and test of the Hermes shuttle

Computations were made of the flow around the Hermes shuttle at $M = 0.2$ for the incidence angles $0 < \alpha < 20°$. As an example, Fig. 8 shows the result of an ECOPAN computation for incidence $\alpha = 10°$ and sideslip $\beta = 10°$. The distribution of the pressure coefficient $C_P$ calculated over the aircraft surface shows that the greatest overvelocities are located near the leading edge on the upper side of the wing profiles farthest outboard, particularly over the winglets, while the regions in compression are located obviously at the nose of the aircraft and over the canopy.

The Figure 9 compares the results of the ECOPAN computations with test results.

The lift coefficient $C_L(\alpha)$ estimate is very good: the calculated curve falls very close to the experimental curve between 0 and 20° of angle of attack.

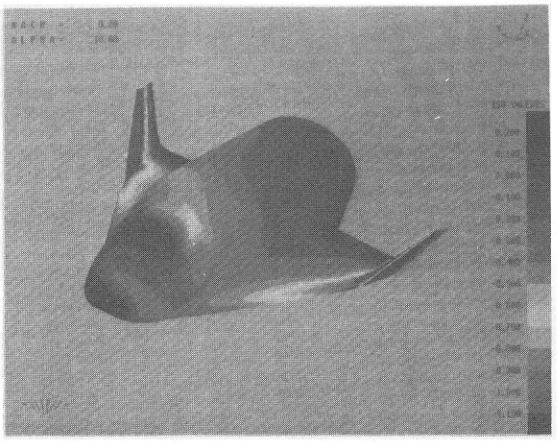

*Fig. 8. ECOPAN pressure field computation on the Hermes shuttle ($M = 0.2$; $\alpha = 10°$; $\beta = 10°$).*

The moment coefficient $C_{M60}$ estimate is less good, particularly the return to the stability observed in the test at incidences above $\alpha = 10°$, and which is not predicted by the ECOPAN computation. However the discrepancies observed between the computation and the test are quite acceptable considering the hypothesis of the calculation (inviscid flow, base flow condition, no wake vortex deformation at high angles of attack and no consideration of leading edge vortex flows).

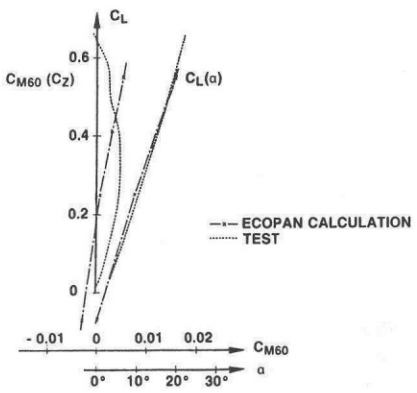


*Fig. 9. Hermes shuttle: comparison of normal force and moment calculation with wind-tunnel data.*

## IV. Ariane 5 applications

Within the framework of the studies of Ariane 5 Technical Assistance for the CNES*, the Aerodynamics Department of ONERA is in charge of evaluating the aerodynamic characteristics of the launch vehicle, by means of computation methods available at ONERA, to determine how different architectural configurations of the automatic and Hermes versions would behave.

First we describe how the surface grid is generated from the geometric definition of the launcher, noting the specific grid generator programs developed as ECOPAN improvements for the needs of the Ariane 5 study case.

The last part is a comparative analysis of the longitudinal aerodynamic characteristics of the launcher at $M = 0.5$ as calculated by ECOPAN and as determined by tests. The automatic and Hermes versions are compared, to evaluate the Hermes effect over the lower part of the launcher.

Surface grid generation

In the case of the Hermes-Ariane 5 configuration, the space plane grid was generated by the available obtained CAD software at ONERA. The rest of the grid (the launch vehicle) was generated by a program developed at ONERA within the framework of the present application, to mesh simple shapes such as spheres, cones, cylinders, etc ... or perform geometric transformations such as rotations, translations or similarity transformations.

The grid of the automatic and Hermes configurations are divided into 10 and 14 sub-domains, respectively.

The modularity and interchangeability of certain parts of the grid make it easier to define different versions of the Ariane 5 launcher. The division into sub-domains also allows partial integrations of the aerodynamic coefficients, at the exit from the ECOPAN processing.

The configuration grids consist of 4278 panels for the automatic version and 5932 for the Hermes version representing half the plane.

---

* Centre National d'Etudes Spatiales, the French space agency

These are shown in the Fig. 10. Note however that:
- Some parts of the grids, such as the booster nose cones and the Hermes adapter, were made more dense, as the wake effects of the Hermes wings are strong in these areas.
- The panels facing each other on the boosters and central body are of the same dimensions, to avoid numerical problems due to the small distance between boosters and central body.

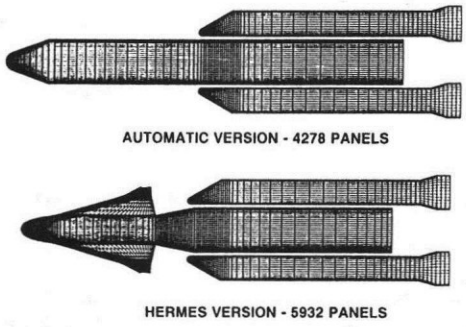


*Fig. 10. Ariane 5 launch vehicle grids for the automatic and Hermes configurations.*

## Wake for the Hermes configuration

### Geometric definition

The trailing edge of the Hermes wing is extended by a thin surface modeling the wake.

The wake geometry, highly distorted by the presence of boosters downstream of the Hermes trailing edge, is taken as unknown. The method used to approach this geometry is the following:
- A first computation is made of the Ariane 5-Hermes composite at zero incidence without the wake (nonlifting computation).
- Streamlines from the Hermes trailing edges are computed by means of a module specially adapted to the ECOPAN code.
- The wake is defined geometrically. The calculated streamlines cannot always be used directly in defining a wake, because we have to make sure that they do not interact directly with the mesh of the boosters. In this particular case, some local corrections may be necessary.

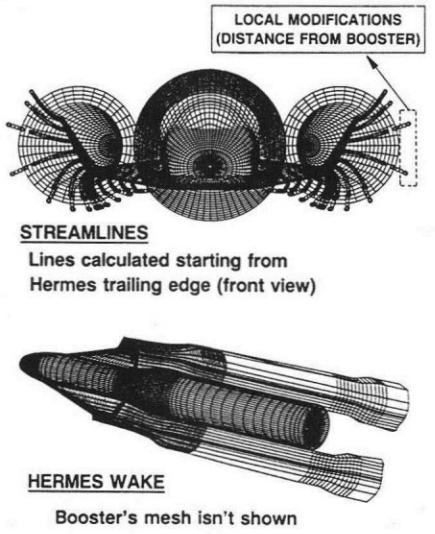


*Fig. 11. Hermes wake sheet geometry.*

An interactive geometric processing code has been written to make this type of local modifications easier.

The Figure 11 illustrates a wake defined this way. The wake grid is drawn tighter around sharp bends and areas of complex geometry (around the cones of the boosters or downstream of the exhaust nozzle) and are extended into the downstream flow by means of panels with high aspect ratio.

### Condition applied to the trailing edge of the Hermes wing

The trailing edge of the Hermes wing is extended by a thin wake made up of doublet panels. Considering the relatively thick wing base, special conditions were needed to express the Kutta-Joukowski condition (see the scheme in Fig. 12).

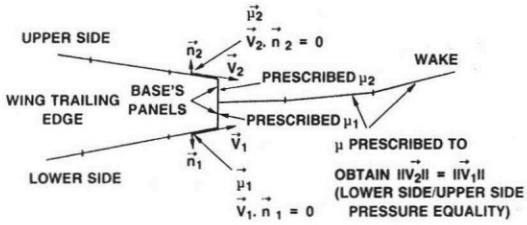


*Fig. 12. Boundary conditions around the Hermes wing trailing edge.*

The wake starts from the middle of the base,its shape being given by a preliminary computation of streamlines.

The base is closed by two doublet panels, whose strengths are determined by those of adjacent trailing edge panels ($\mu_1$ and $\mu_2$, see Fig. 12). The doublet strength over the wake is found by iterating until the pressures on the upper and lower sides of the trailing edge are equal.

### Special precaution

The first wake lattice, at the wing root, has to run along a grid line over the adapter and the central body. For the velocity calculation to be correct along this grid line, the surfaces to either sides (Fig. 13) have to be separated.

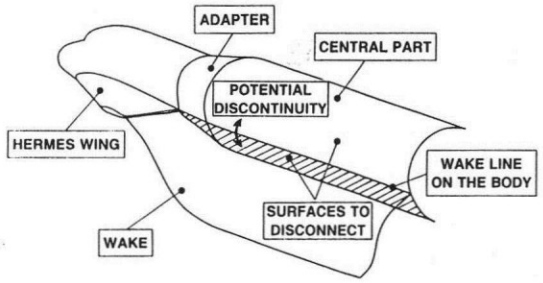


*Fig. 13. Schematic representation of the junction between the Hermes wake and the central body.*

The velocities are obtained by the gradient of the doublet distribution, which must remain unchanged by the potential jump due to the wake presence.

## Base lattices

### Geometric definition

Wake lattices are also used to model the base areas of the boosters and central body (see Fig. 14). Downstream of the boosters, the lattices extend the base by a cylinder. The lattice from the central body base contracts to avoid the booster exhaust nozzles.

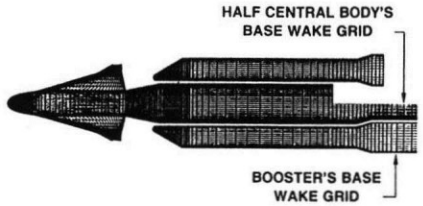


*Fig. 14. Booster and central body base: geometric definition of wake lattices.*

### Conditions applied on the base wakes

To attenuate the interaction effects observed during the preliminary study, a base flow condition was developed, using wakes without any slip condition. This type of wake is better than the extension of the grid by solid surfaces of the cylindrical model-support sting type. However, the slip condition ($\vec{V}.\vec{n} = 0$), which is commonly used to model the separated area downstream of a base, yields satisfactory results for simple configurations like isolated boosters.

In the case of the Ariane 5 launcher, on the other hand, the central body base is located upstream of the booster exhaust nozzles, so the grid geometry in the continuation of the central boby can thus strongly modify the aerodynamics of the lower parts as the boosters.

This problem was solved as follows:
The base wakes are made up, of doublet panels alone. We impose a constant gradient, in the longitudinal direction (upstream to downstream).

The unknowns are thus, the value of the gradient and the doublet strengths over every panel at the foot of the wake.

The condition imposed[16] is a velocity minimization (for the modulus) over the base panels adjacent to the lattice (see the scheme in Fig. 15).

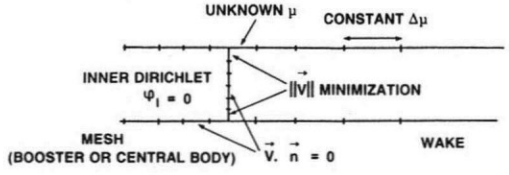


*Fig. 15. Boundary conditions on the base region.*

This type of condition imposes fewer constraints on the flow downstream of the base. A test with an isolated P170 booster has actually shown that streamlines sometimes run across the wake, which cannot be simulated, of course, with a "solid sting".

## Computation results

All the versions were computed at $M = 0.5$, for two incidences: $\alpha = 0°$ and $\alpha = 3°$.

The Mach number was voluntarily limited to 0.5, because the compressibility correction of Prandtl-Glauert type used in the code cannot take transonic effects into account.

The Hermes configuration was computed with a "prescribed wake", that is without any iteration on the wake geometry. The same wake geometry is used for the two incidences, which is acceptable in so far as the incidence is limited to values around zero.

Note that it will be possible to consider computing a free-wake geometry (iteratively), at the cost of some additional computation time and a drawing tighter in the spanwise direction for the mesh fineness of the Hermes wing.

ECOPAN computation results for $M = 0.5$ have been used to characterize the effects changing the upper "payload" part has on the launcher performance, by comparing automatic and Hermes versions.

### Pressure distributions

The plot of the pressure distributions computed over the two versions (Fig. 16) shows a major change when the upper part changes, located mainly at the level of booster cones. For the Hermes version, the slope jump at the adapter - central body junction is expressed by overvelocities in this zone by comparison with the automatic version. The effect of the space shuttle wake is clearly seen along the boosters (differences in the constant-$C_P$ field in Fig. 16) but seems to be moderate enough over the cylindrical parts.

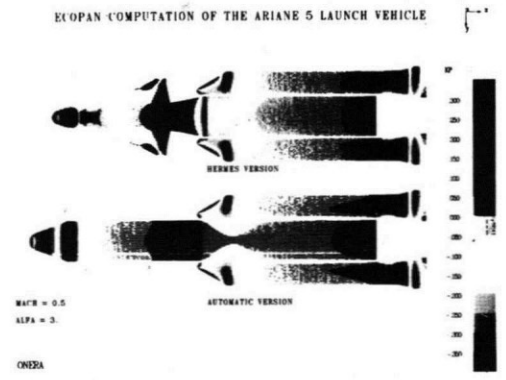


*Fig. 16. Ariane 5 launch vehicle: ECOPAN computation of the pressure field.*

### Longitudinal coefficient

The longitudinal aerodynamic coefficients of the two versions are shown in Fig. 17a and b. The normal force coefficients ($C_N(\alpha)$, Fig. 17a) and moment coefficients about the center of gravity ($C_M(\alpha)$, Fig. 17b) are solved over the upper part (Hermes and adapter or fairing, depending on the version) and the lower part (central body and boosters).

The change from the automatic version to the Hermes version is expressed, in terms of normal force coefficient level, by an increase in the global normal force coefficient gradient of $\Delta C_{N\alpha} = 0.069$ (that is, 54.8 % of the global $C_{N\alpha}$ for the automatic version).

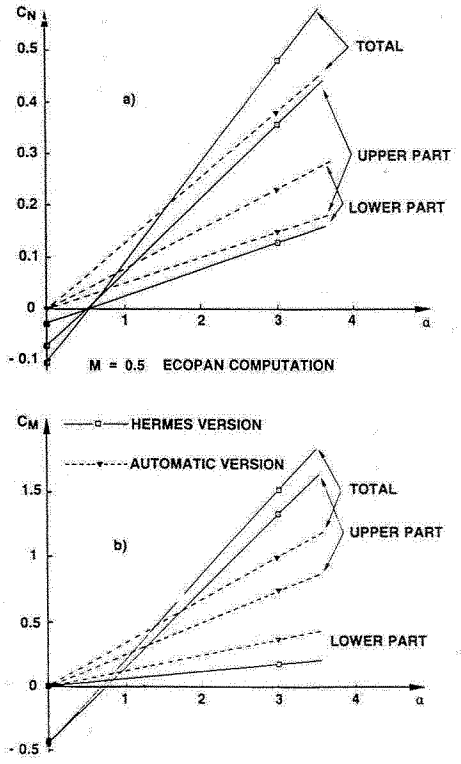


*Fig. 17. Ariane 5 launch vehicle: normal force and moment computation.*

If we consider the weighed force of the upper part, we note that the difference in the slopes is higher than this ($\Delta C_{N\alpha}=0.094$, i.e. 74.4 % of the global $C_{N\alpha}$). The increase in normal force coefficient of the upper part is thus partly compensated by an inverse effect on the lower part.

In terms of moment coefficients about the center of gravity (Fig. 17b), the decreasing of stability due to the presence of Hermes is expressed by a high increase in the gradient of the global moment coefficient: $\Delta C_{M\alpha}=0.322$ (i.e. 96.8 % of the global $C_{M\alpha}$ for the automatic version).

As in the previous case, the difference in the $C_{M\alpha}$ for the upper part is higher than the global difference ($\Delta C_{M\alpha}=0.344$ or 103 % of the global $C_{M\alpha}$), the difference corresponding to the lower part with less compensation than for the normal force coefficients.

The change from the automatic version to the Hermes version thus results in a decrease of the launcher total stability, due to the higher normal force coefficient of the upper part of the Hermes version. This decrease is moderated by a favourable interaction of Hermes wake on the lower part of the launcher which must now necessary to qualify more precisely.

Effect of Hermes over the lower part of the launcher

The disturbance of the aerodynamic field on the lower part of the launcher was studied on the normal force coefficient distributions (for $\alpha=3°$) on the boosters and central body of both the automatic and the Hermes versions. On the boosters (Fig. 18a) we note a high decrease in lift on the sloping cones ( $20\,m<X<25\,m$) due to the presence of Hermes. The effect can be neglected on the cylindrical part but becomes noticeable again at the level of the booster exhaust nozzles ($48\,m<X<50\,m$). On the lower part of the central body (Fig. 18b) the lift decreasing is concentrated under the adapter-central body junction ($21\,m<X<23\,m$); no effects are visible further downstream.

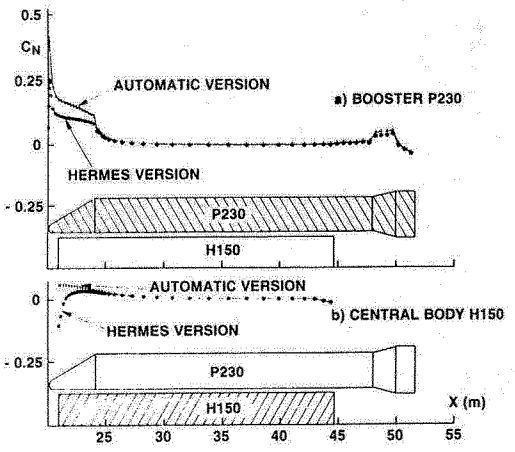


*Fig. 18. Longitudinal normal force distribution on lower part of launch vehicle.*

A calculation of the Hermes version at $\alpha=3°$ but without wake, not presented in this paper, showed how much of the downstream aerodynamic disturbance was due to the Hermes wake and how much to the adapter.

In the case of the central body, the unlifting effect is induced by the adapter and not by the wake. The Hermes version calculations with and without wake show the same effect. In the case of the boosters, the interaction effect is induced by the wake vortex sheet starting from the Hermes wing: the differences between the automatic and Hermes versions, on the one hand, and the Hermes versions with and without wake, on the other, are practically the same.

Comparison with test results

Tests conducted at the NLR on the automatic and Hermes versions at Mach 0.8 were also analysed to characterize the interactions.

The test assembly with models equipped with three balances weighs separately the upper part (nose fairing or Hermes and adapter, depending on the version), one isolated booster and the central part of the launcher (upper part and central body).

The normal force gradients (calculated between 0° and 3° of incidence) deduced from test results at $M=0.8$ and from computations at $M=0.5$ are presented in Table I. The weighed force of the lower part (LP) of the launcher (boosters and central body H150 located under the adapter) is deduced from the total (TOT) weighed force for either versions.

A comparison of the interaction effect of Hermes on the lower part of the launcher between these two different Mach numbers have been made for the following reasons:
- For the two cases there are not large transonic zones. In the range of incidences investigated ($0\leq\alpha\leq3°$), the residual transonic effects have not considerable influence on the interaction.
- At the time of the comparison no test results were available at $M=0.5$

| | Calculation $M=0.5$ | | Test $M=0.8$ | |
|---|---|---|---|---|
| Version | Auto | Hermes | Auto | Hermes |
| $C_{N\alpha}\,TOT$ | 0.1263 | 0.1955 | 0.1944 | 0.2315 |
| $C_{N\alpha}\,LP$ | 0.0767 | 0.0522 | 0.1423 | 0.01043 |
| $\Delta C_{N\alpha}\,LP$ | -0.0245 { -0.0240 boost. / -0.0005 H150 | | -0.0380 { -0.0256 boost. / -0.0124 H150 | |
| $\frac{\Delta C_{N\alpha}\,LP}{C_{N\alpha}TOT_{Auto}}$ | -19.4 % | | -19.5 % | |

*Table I. Normal force gradients performed by calculation and test for the two launcher configurations.*
*Note: $\Delta C_{N\alpha}$: difference between Hermes and automatic versions.*

The lift decrease on the lower part of the launcher, revealed by the calculation is also present in the test results ($\Delta C_{N\alpha}\,LP$, Table I). The greatest effect is located on the boosters, with a good agreement between computation and tests. Over the central body H150, the computed effect is smaller than in the test results. The total difference on the lower part ($\Delta C_{N\alpha}\,LP$) is 19.5 % of the total normal force gradient for the automatic version, in the tests, and 19.4 % in the calculation (see Table I).

The good agreement between calculation and test, although the Mach numbers are different, validates the use of the ECOPAN code for the calculation of interaction effects.

Interpretation of interaction effects due to Hermes

The difference between the normal force gradients on the lower part of the launcher for the automatic and Hermes versions ($\Delta C_{N\alpha}\,LP$, Table I) is expressed in terms of the relative interaction of the flow from the Hermes wing by:

$$\frac{\Delta C_{N\alpha}\,LP}{C_{N\alpha}\,LP_{Auto}}$$

To characterize the increasing stability or decreasing stability due to the interaction, we can estimate the position of the aerodynamic center of the interaction effect from Hermes on the lower part by:

$$Xf = Xm - \frac{\Delta C_{M\alpha}\,LP}{\Delta C_{N\alpha}\,LP} \times L\,ref.$$

with $Xm$ = position of the center of gravity: moment calculation point.
$Lref.$ = central body H150 diameter.

The values of the interactions as well as the corresponding center position, evaluated from NLR tests and ECOPAN computations, are given in the following Table II:

| | Calculation $M=0.5$ | Test $M=0.8$ |
|---|---|---|
| $\Delta C_{N\alpha}\,LP$ | -0.0245 | -0.0380 |
| $\frac{\Delta C_{N\alpha}\,LP}{C_{N\alpha}\,LP_{Auto}}$ | -32 % | -27 % |
| *Xf/Hermes nose* | 28.13 m | 28.18 m |

*Table II. Characterization of the interaction effect from Hermes to lower part.*

We note the good agreement between the computation and the tests concerning the interaction center positon. These positions shown in Fig. 19 locate the interaction center 4.9 m above the center of gravity of the launcher (computation and test averaging): this effect contributes to limit slowly the decreasing of stability effect due to the upper part itself (Hermes and adapter).

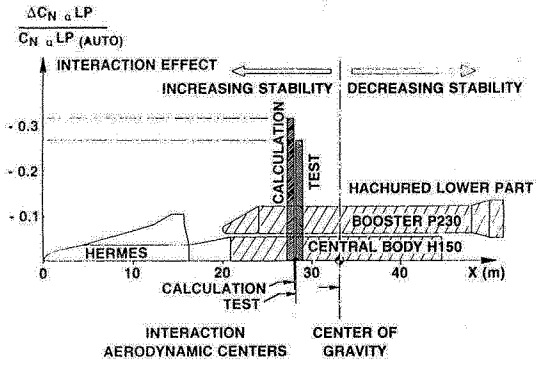


*Fig. 19. Hermes interaction effect on lower part of launch vehicle.*

## IV. Airbus aircraft applications

The ECOPAN code was delivered to Aerospatiale under the terms of an SPTA* research contract for transport aircraft studies.

The first aircraft geometries studied were very simply with wing-fuselage type configurations and simplificated wake geometries.

Preliminary configuration investigated: wing-fuselage configuration with prescribed wake sheet

A wing-fuselage configuration was quite appropriate for testing the method, particularly to verify the computation in the wake sheet-fuselage interaction zone.

The mesh of the wing in the presence of an Airbus type fuselage, which satisfies the constraint of regular closure at the trailing edge, in order to assure a good junction with the wake sheet, came from the Aircraft Division of Aerospatiale. The wing-fuselage grid set consists of 1537 panels.

* "Service Technique des Programmes Aéronautiques" of the French Defence Ministry

A prescribed wake lattice was defined next, with 510 panels: it starts along the trailing edge bisector of the wing along the line of the freestream velocity direction. Along the fuselage, the lattice is attached to a grid line corresponding approximately to a streamline, thereby making a relatively airtight junction.

A view of the whole grid is shown in Fig. 20, along with this wake lattice. This was used as input for the ECOPAN code.

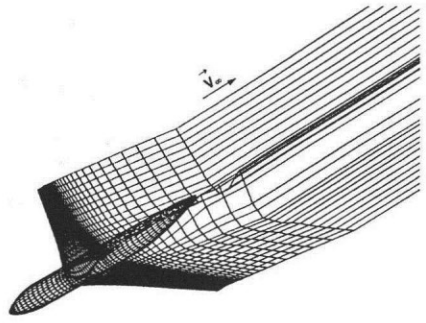

*Fig. 20. Grid of a wing-fuselage configuration with wake lattice.*

The Fig. 21 graphs an intermediate computation giving the doublet strength distribution over the surface, clearly showing the potential jump induced by the wake lattice along the fuselage.

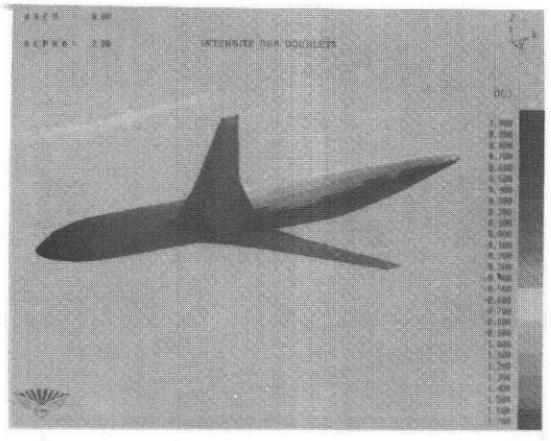

*Fig. 21. Doublet strength field on the wing-fuselage configuration.*

The pressures are then calculated from the surface gradients of the potential, and more precisely of the doublet strengths, taking into account the absence of coupling between the domains located to either side of the discontinuity line on the fuselage.

This potential jump induces no noticeable pressure discontinuity.

However, there was one local defect in the first configuration studied, at the level of the fuselage base flow. This has been corrected since; but we show it here as an example in Figure 22.

Later developments in the ECOPAN code have made it possible to correct this type of defect and to consider much more complex and realistic geometries.

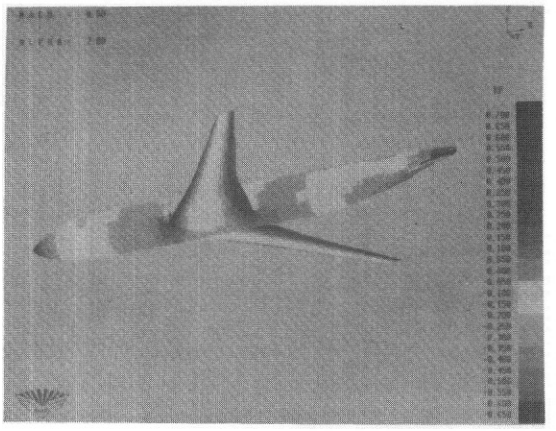

*Fig. 22. Pressure coefficient field on the wing-fuselage configuration.*

Computation of a complete aircraft in takeoff configuration

Computations of complete aircraft in takeoff configurations with flaps and slats extended requires industrially operational codes. On request from Aerospatiale, the ECOPAN code was evaluated on an Airbus geometry in just such a configuration.

The grid developed by Aerospatiale consists of 10250 panels representing half the airplane. The wake sheets from the lifting surfaces (wing, leading edge slat, flaps and tail section) comprise 5800 doublet panels, with the various tip vortices being modeled by rolling up the wake sheets (Figs. 23 and 24).

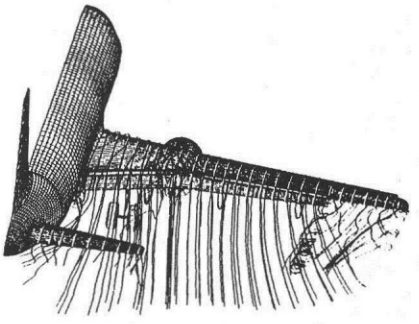

*Fig. 23. Rear view of the Aerospatiale Airbus grid - 10250 panels.*

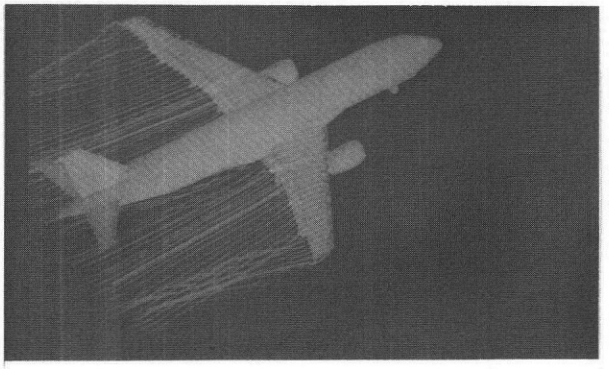

*Fig. 24. Airbus grid of 10250 panels seen from above.*

These lattices were generated on the basis of an initial flow streamline calculation, without any later calculation of a free-wake geometry.

The engine primary and secondary fluxes are simulated by setting a normal velocity condition at the engine face section and an exhaust condition on the engine outlet section panels (Fig. 25).

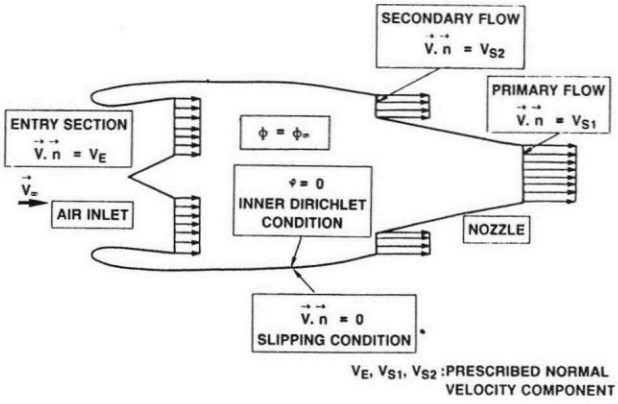


*Fig. 25. Simulation of engine primary and secondary fluxes.*

A pressure distribution calculated in the presence of wake lattices and engine jets is shown in Fig. 26.

To simulate the ground effect on the aircraft, an implicit plane of symmetry is located at ground distance. The corresponding calculated pressure distribution is presented in Fig. 27 and Fig. 28.

*Fig. 26. Airbus front view with wake representation used for the computation.*

Both these pressure distributions show that the ECOPAN computation code has operated well on such a configuration: no particular numerical problems have been detected in the strong wake-fuselage interaction zones.

The upper side view in Fig. 27 clearly shows a high suction at the leading edge, at the level of extended slats. This confirms that the high lift devices, operating in this takeoff configuration, are well simulated.

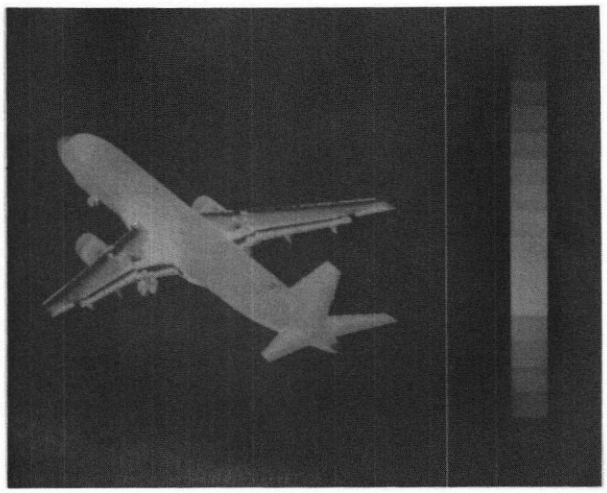

*Fig. 27. Pressure field on Airbus type aircraft: ECOPAN calculation with ground effect.*

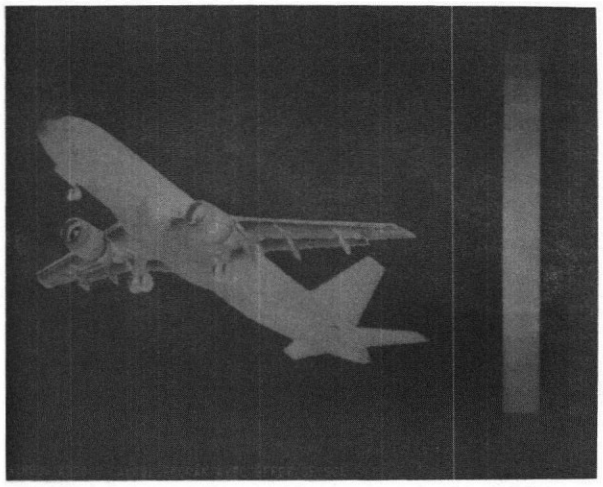

*Fig. 28. Pressure field seen from underneath: ECOPAN calculation with ground effect.*

The wakes generated from the leading edge slats are very close to the wing upper side and do not create any numerical problems.

The pressure distributions were generated in a takeoff configuration with and without a plane of symmetry. By integrating both these pressure distributions, the ground effect can be estimated to be of the order of a 4 % increase in lift for this computation case, which is in agreement with the flight test results.

These results show that the ECOPAN code is operational. However, this preliminary calculation performed with a prescribed wake geometry does not permit to assert that this code is able to determine the entire ground effect configurations presently.

Nevertheless, some improvements could be made, such as a complete free-wake geometry calculation.

One encouraging free-wake geometry calculation has been performed in a two-dimensional configuration on a wing profile of this aircraft.

The Figure 29a presents the streamline calculation with a visualization of the estimated wake used as input for the calculation, and the Figure 29b the result after the second free-wake geometry iteration.

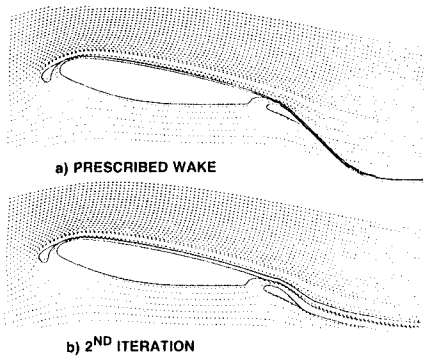


*Fig. 29. Free-wake geometry calculation - Two-dimensional configuration.*

## V. Conclusion

The results presented demonstrate that the ECOPAN singularity code is an operational code for calculation of inviscid subsonic flows around a large variety of complex three-dimensional configurations, including those of a complete aircraft or launch vehicle.

This code, which was developed for various uses in aerodynamics or flight mechanics, can calculate the:
- velocity, pressure and Mach number fields in the flow or on the body surface,
- streamlines in the flow,
- local and global force and moment estimations, by integrating the pressures over the bodies.

The computation times depend, of course, on the fineness of the grid and thus on the accuracy required, but are generally relatively short, which make parametric analyses possible.

The ECOPAN code has thus demonstrated its versatility and operational status in a broad field of application.

Our comparative analysis of the automatic and Hermes versions of the Ariane 5 launch vehicle has drawn out the most significant geometric effects on the longitudinal stability of the launcher.

The study has shown that ECOPAN can determine differences in the longitudinal aerodynamic coefficient between the two Ariane 5 versions that are realistic, compared with the test results.

The ECOPAN code also correctly expresses the interactions of the Hermes shuttle with the lower part of the Ariane 5 launcher.

The comparative analysis of the forces applied to a complete aircraft in takeoff configuration with and without a plane of symmetry simulating the ground effect, permitted to estimate the corresponding increase in lift.

As a conclusion, the ECOPAN code is particularly well adapted to parametric analyses in subsonic flow.

These conclusions, limited to inviscid flow, could be extended for use in those cases where the viscous effects cannot be neglected, by:
- taking boundary layers into account using transpiration velocities,
- better expression of separated base flows,
- better wake simulation in the presence of lifting fuselage,
- inclusion of free-wake lattice geometry calculation,
- possibly a better way of taking compressibility effects into account.

## References

1. KIRRMANN C.: "Comparaison de différentes méthodes de singularités pour le calcul des écoulements internes en tridimensionnel". 11e Colloque d'Aérodynamique Appliquée AAAF - Ecully (1984), and TP ONERA 1984-150.

2. MARGASON R.J., KJELGAARD S.O., SELLERS W.L., MORRIS C.E.K., WALKLEY K.B., SHIELDS E.W.: "Subsonic Panel Methods - A Comparison of Several Production Codes". AIAA Paper No 85-0280, January 1985.

3. STRANG W.Z., BERDAHL C.H., NUTLEY E.L., MURN A.J.: "Evaluation of Four Panel Aerodynamic Prediction Methods (MCAERO, PAN AIR, QUADPAN and VSAERO)". AIAA Paper No 85-4092, October 1985.

4. CLARK D.R., MASKEW B., DVORAK F.A.: "The Application of a Second Generation Low-Order Panel Method - Progam VSAERO - to Powerplant Installation Studies". AIAA Paper No 84-0122, January 1984.

5. ROSS J.C.: "Applicability of a Panel Method, which Includes Nonlinear Effects , to a Forward-Swept-Wing Aircraft". AIAA Paper No 84-2402, October, November 1984.

6. SMITH B.E., ROSS J.C.: "Application of a Panel Method to Wake Vortex/Wing Interaction and Comparison with Experiment". AIAA Paper No 84-2182, August 1984.

7. STRASH D.J., NATHMAN J.K., MASKEW B., DVORAK F.A.: "The Application of a Low-Order Panel Method - Program VSAERO - to Powerplant and Airframe FLow Studies". AIAA Paper No 84-2178, August 1984.

8. LIU T.M., SCHAEFER R.W.: "A Comparative Study of Computer Codes for Flow Field Calculation of Nacelle Inlets". AIAA Paper No 86-0397, January 1986.

9. MIRANDA L.R.: "Application of Computational Aerodynamics to Airplane Design". AIAA Paper No 82-0018, January 1982.

10. BASTON A., LUCCHESINI M., MANFRIANI L., POLITO L., LOMBARDI G.: "Evaluation of Pressure Distributions on an Aircraft by Two Different Panel Methods and Comparison with Experimental Measurements". ICAS Paper No 86-1.5.3, September 1986.

11. FORNASIER L., HEISS S.: "Application of HISSS Panel Code to a Fighter-Type Aircraft Configuration at Subsonic and Supersonic Speeds". AIAA 5th Applied Aerodynamics Conference, August 17-19, 1987, Monterey, California.

12. SNYDER L.D., ERICKSON L.L.: "PAN-AIR Prediction of NASA Ames 12-Foot Pressure Wind Tunnel Interference on a Fighter Configuration". AIAA Paper No 84-0219, January 1984.

13. CONNER R.S., PURDON D.J.: "PAN-AIR Knowledge System". AIAA Paper No 86-0239, January 1986.

14. BOILLOT H., LE T.H.: "Asynchronous I/O Technics and Block Management". 1st World Congress on Computational Mechanics, University of Texas, Austin, September 22-26, 1986.

15. CARR M.P.: "Accuracy Study of Transonic FLow Computation for 3D Wings". AGARD CP 437, May 1988.

16. LE T.H., RYAN J., FALEMPIN G.: "Wake Modeling for Helicopter Fuselages". 13th European Rotorcraft Forum, Arles, France, September 1987 and TP ONERA 1987-145.